A VUV Photoionization and Ab Initio Determination of the Ionization Energy of a Gas Phase Sugar (Deoxyribose).

Debashree Ghosh[1], Amir Golan[2], Lynelle K. Takahashi[2,3], Anna Krylov[1], and Musahid Ahmed[2*]

[1]Department of Chemistry, University of Southern California, Los Angeles, CA 90089-0482

[2]Chemical Sciences Division, Lawrence Berkeley National Laboratory, Berkeley, CA 94720

[3]Department of Chemistry, University of California at Berkeley, Berkeley, CA 94720

*Corresponding author: MS: 6R-2100, Lawrence Berkeley National Laboratory, 1 Cyclotron Road,

Berkeley, CA 94720, USA. Phone: (510) 486-6355; fax: (510) 486-5311; email: MAhmed@lbl.gov

Abstract- The ionization energy of gas-phase deoxyribose was determined using tunable vacuum ultraviolet synchrotron radiation coupled to an effusive thermal source. Adiabatic and vertical ionization energies of the ground and first four excited states of α-pyranose, the structure which dominates in the gas phase, were calculated using high-level electronic structure methods. An appearance energy of 9.1(±0.05) eV was recorded which agrees well with a theoretical value of 8.8 eV for the adiabatic ionization energy. A clear picture of the dissociative photoionization dynamics of deoxyribose emerges from the fragmentation pattern recorded using mass spectrometry and from ab initio molecular dynamics calculations. The experimental threshold (9.4 eV) for neutral water elimination upon ionization is captured well in the calculations, and qualitative insights are provided by molecular orbital analysis and molecular dynamics snapshots along the reaction coordinate.

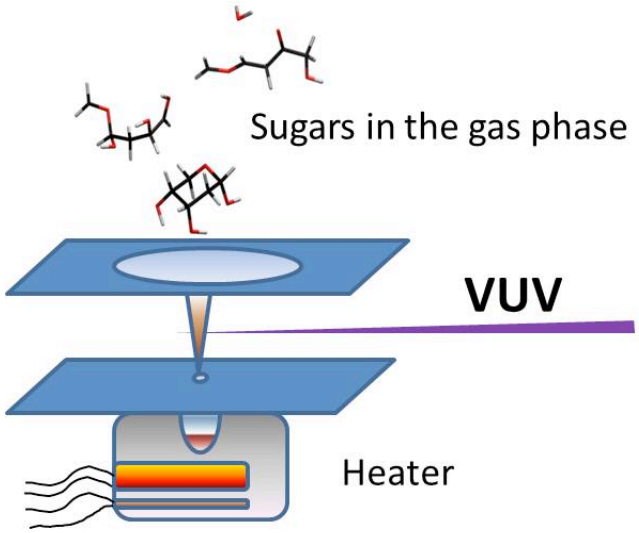

Keywords: sugars, synchrotron radiation, electronic structure calculations, mass spectrometry, fragmentation.

Sugars, together with phosphates, constitute the scaffold on which nucleic acids build up DNA's structure. 2-deoxy-D ribose, the "D" in DNA, exists predominantly in the pyranose form in the aqueous phase, and it is believed to maintain this structure in the gas phase too.[1] The interaction of energy (X-rays, electrons, particles, VUV photons) with DNA has been studied in detail over a number of years, yet some basic questions regarding the electronic structure of the building blocks of DNA remain unanswered.[2,3] For example, a question such as "what is the ionization energy of deoxyribose?" does not generate a number with much certainty. There is one report in the literature of a 10.5 eV ionization energy measured using electron ionization,[4] and a few theoretical calculations present numbers around this value.[5-8] This is a surprisingly high value for a molecule that contains oxygen in a ring structure. Similar molecules such as tetrahydrofuran have ionization energies much lower, and there is near perfect agreement between theory and experiment for that molecule.[9,10] There have also been a number of experimental and theoretical[11,12] studies on the fragmentation of deoxyribose molecules from energetic radiation. However, these have often relied on an ionization energy of 10.5 eV or higher for the parent molecule to explain the experimental results.[4-6,13] The difficulty in generating an experimental ionization energy for sugars such as deoxyribose stems from the difficulty to prepare intact molecules in the gas phase for subsequent interrogation by ionizing radiation.

In this study we employ a gentle thermal desorption method coupled to tunable VUV photoionization to measure an experimental ionization energy for deoxyribose and to study its fragmentation mechanisms. We compare the experimental measurements with electronic structure calculations of vertical and adiabatic ionization energies. Ab initio molecular dynamics (AIMD) simulations are used to understand different fragmentation channels obtained via dissociative photoionization. The results and techniques described here will aid in a general understanding of the electronic structure of sugars, a topic of much discussion recently since biofuels are been seen as 21st century transportation fuels.[14] There is great interest in understanding the thermal and photoionization dynamics of molecules such as cellulose, levoglucosan, glucose, and cellobiose, among other molecules.[15,16] Our group has started a systematic program to study the photoionization and desorption dynamics of biomolecules,[17,18]

sugars and other lignocellulosic[19] material using a variety of experimental and theoretical methods, and here, to the best of our knowledge, we present the first experimental photoionization energy measurement for deoxyribose and an accurate calculated value of its ionization energy.

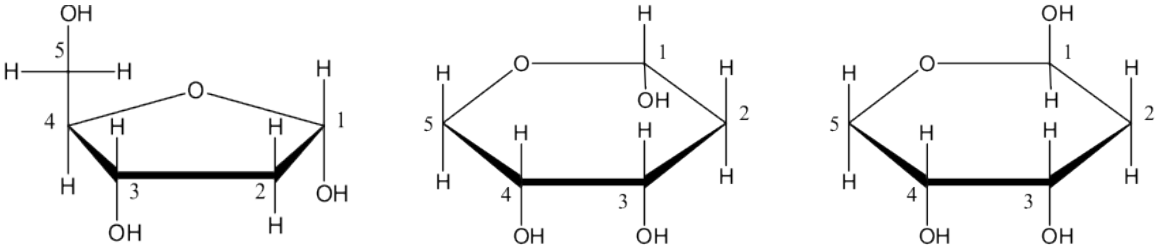

(a) Furanose (b) α Pyranose (c) β Pyranose

Figure 1: Structures of furanose, α pyranose and β pyranose form of 2-deoxy-D-ribose.

The relative energies of the pyranose and furanose forms of 2-deoxy-D-ribose are shown in Table 1. The pyranose form is 7.9 kcal/mol lower than furanose in the gas phase. Thus, although furanose is the most common form in DNA, pyranose is the most abundant form in the gas phase. The pyranose structures have two isomers (α and β) depending on the OH group position in C_1. The α structure has the OH group pointing down in the Fischer diagram and β structure has the OH group pointing up. The α structure is more stable by 5.6 kcal/mol than the β form.

Table 1: Relative stability of the gas-phase furanose and pyranose forms computed by DFT/ωB97x/cc-pVTZ

Species	Rel. energy in kcal/mol
Furanose	7.90
α-Pyranose	0.0
β-Pyranose	5.60

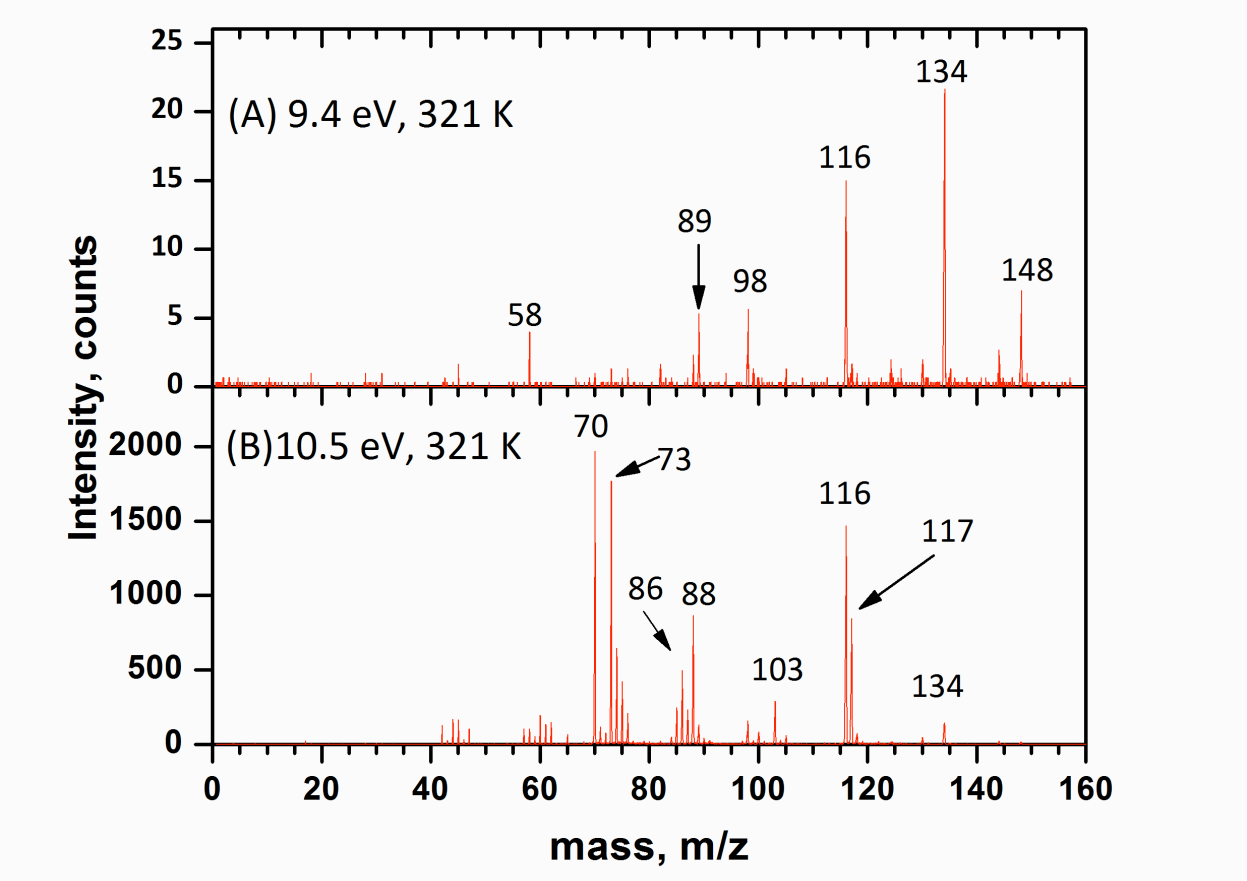

Figure 2: Experimental mass spectrum of deoxyribose gas-phase molecules recorded using an effusive source maintained at 321K and at (a) 9.4 eV and (b) 10.5 eV, respectively.

Figure 2 (A) shows a mass spectrum of deoxyribose recorded at a photon energy of 9.4 eV. The main peak at m/z 134 corresponds to the deoxyribose cation. The next major peak is at 116 amu and arises from the elimination of H_2O, while other peaks are seen at 58, 89, 98 and 148 amu. Upon increasing the photon energy to 10.5 eV (Fig. 2(B), the parent signal decreases dramatically, and m/z 70 and 73 along with 116 amu dominate the spectrum. A new peak at 117 amu is also prominent. The m/z 148, 98 and 88 features are tentatively assigned to methyl-deoxyribose, furfural alcohol and tetrahydrofuranol by comparing photoionization efficiency curves (PIEs) to reported ionization energies and the measured PIE of deoxyribose in this work (see supplementary material, SM). The m/z 103 and 116 features arise from elimination of CH_3O and H_2O respectively. Extensive fragmentation has been noted from deoxyribose, upon electron

ionization,[4] VUV ionization,[13] and particle bombardment.[6] The mass fragments at m/z 70, 73, 88, 103, 116 and 117 amu have been observed under these conditions, but very little or no parent cation (m/z 134) has been observed in these earlier experiments. In a previous VUV photoionization study of deoxyribose,[13] the parent mass at m/z 134 was not detected, and there was extensive fragmentation, similar to a 70 eV electron ionization mass spectrum. Recently Shin et al.[5] laser desorbed a deoxyribose/R6G mixture and using 26.44 eV laser photons saw extensive fragmentation similar to that seen in earlier work using electron impact and VUV ionization and no evidence for the parent cation. In our case, thermal desorption at lower temperatures (303-323 K) should give rise to less decomposition and ionization at threshold allows for detection of the parent cation.

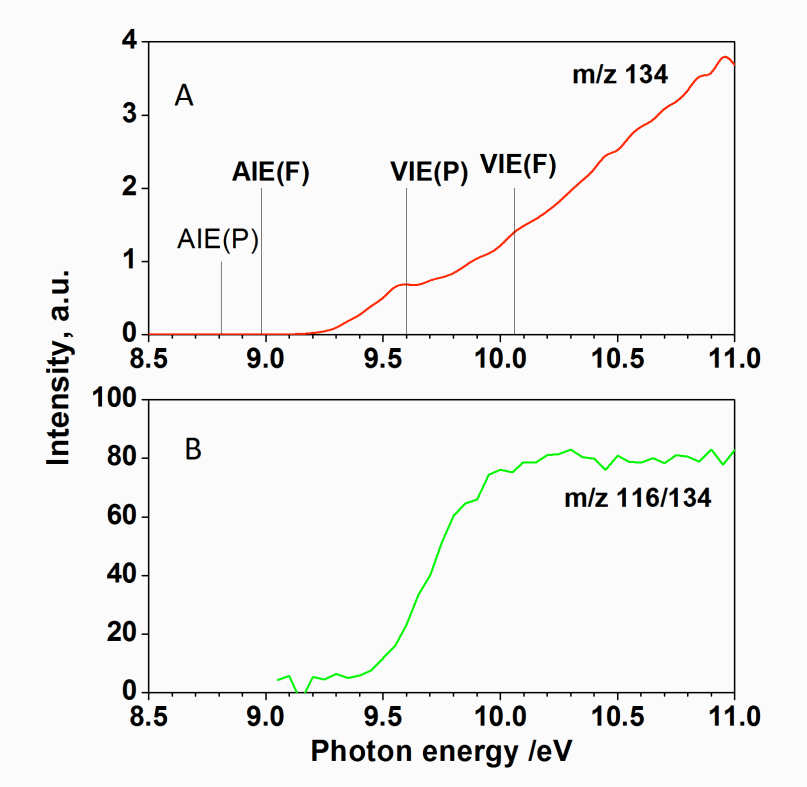

Figure 3: (A) An experimental PIE curve for deoxyribose recorded with a step size of 50 meV. The vertical lines denote calculated adiabatic (AIE) and vertical (VIE) ionization energies of the furanose (F) and pyranose (P) forms of deoxyribose, respectively. (B) A PIE curve for m/z 116 (water elimination channel) normalized to parent mass at m/z 134.

The computed (ωB97x/cc-pVTZ**)** gas-phase ionization energies (vertical and adiabatic ionization energy —VIE and AIE) of the 2-deoxy-D-ribose are given in Table. 2. The IEs for the α-pyranose form were benchmarked against equation-of-motion coupled-cluster with singles and doubles (EOM-IP-CCSD) using cc-pVTZ, and the differences were less than 0.05 eV.

Table 2: Vertical and adiabatic ionization energies of 2-deoxy-D-ribose (in eV) computed by ωB97x/cc-pVTZ.

Species	VIE	AIE w/o ZPE[a]	AIE w/ ZPE[a]	Koopmans VIE
Furanose	10.06	9.05	8.98	10.15
α-Pyranose	9.60	8.86	8.81	9.71
β-Pyranose	9.63	8.74	8.70	9.71

[a] Zero point energy

Both the α and β forms of pyranose deoxyribose have very similar IEs, while the furanose form has higher IE. The AIE with ZPE for α-pyranose is calculated to be 8.81 eV (8.86 without zero point energy (ZPE)) and agrees well with our measured appearance energy of 9.1 eV shown in the PIE curve for the parent mass in figure 3 (A). The discrepancy of 0.2 eV between theoretical and experimental values is likely to be due unfavorable Franck-Condon (FC) factors (FCFs); similar magnitude difference between 00 transitions and the computed apparent PIE onset has been observed in our previous study of thymine-water clusters[20]. The PIE shown in figure 3 (A) rises gradually up to 9.55 eV, plateaus for 0.1 eV, and then continues rising up to 11.00 eV. Our calculated VIE of 9.60 eV suggests poor FCFs for ionization. Experimentally, this manifests as the broad onset in the PIE shape as opposed to a sharp step function. Attempts were made to calculate the FCFs and to generate a photoelectron spectrum using the ezSpectrum code[21] (based on double-harmonic approximation), which has been successfully applied to compare experimental and theoretical results for thymine, thymine clustered with water, and other nucleobases.[22,23] Contrarily to previous studies[22,23], the shape of the computed PIE curve did not agree with the experimental one, most likely due to significant ionization-induced distortions and anharmonic effects one would expect for such a floppy molecule as deoxyribose.

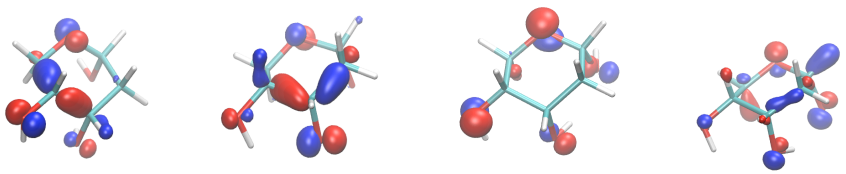

(1) 9.60 (2) 10.51 (3) 11.04 (4) 11.30

Figure 4: Molecular orbitals and vertical ionization energies (in eV) for the lowest 4 ionized states in the α pyranose form of deoxyribose. The EOM-IP-CCSD/cc-pVTZ amplitudes for these orbitals are 0.95, 0.92, 0.92, and 0.93, respectively, revealing dominant Koopmans character of the ionized states.

The molecular orbitals (MOs) giving rise to the first 4 lowest-energy ionized states are shown in Figure 4. These computed EOM-IP-CCSD/cc-pVTZ ionization energies (VIEs are 9.60, 10.51, 11.04, 11.30 eV) suggest that the 2nd ionization onwards will contribute to the rise of signal in the experimental curve only beyond 10 eV. Thus, these states will not be discussed further. Future photoelectron or ion-electron coincidence experiments should allow these ionizations to be followed experimentally. The MO from which the 1st ionization occurs has significant electron density in the oxygen lone pairs, lp(O), and on the bonding σ orbitals between C_3-C_4 and C_4-C_5. The shape of this MO along with the distribution of the spin density (included in SM) explains the observed (in calculations) weakening of the C_4-C_5 bond in the cationic species (1.84 Å versus 1.53 Å in the neutral). Details of the structural changes of the cationic species are given in the SM.

Around 9.4 eV, one of the major fragments is mass 116, which arises from the elimination of H_2O from the parent. At 10.5 eV, the parent signal is low, while m/z 116 remains strong. To disentangle the signal arising from thermal dissociation of deoxyribose, and subsequent photoionization of the fragment and dissociative photoionization, we recorded the PIE for m/z 116. This signal was normalized to the parent mass at m/z 134 to show relative trends and amplify the increase of m/z 116 relative to parent, and the result is presented in figure 3 (B). There is a flat signal of around 5 counts to 9.4 eV and then the intensity rises rapidly and levels off at 10.2 eV with around 80 counts. This independent behavior of the ion signal versus photon

energy suggests the signal prior to 9.4 eV arises from thermal decomposition and the appearance energy at 9.4 eV arises from dissociative photoionization.

While the FC calculations (see SM) were not successful in reproducing the experimental PIE curve, they do aid in understanding the fragmentation mechanisms. The examination of the simulated photoelectron spectrum shown in figure 2 of SM reveals that the ν_2, ν_6, ν_8, ν_{11}, ν_{15}, ν_{21}, ν_{23}, ν_{35} modes are FC active. The largest displacement is along the ν_{11} mode (CH bending around C_2 and C_3, and twist along the C_5O bond in the ring); the overtones or combination bands of ν_{11} give rise to the dominant progression. The other important normal modes are ν_0, ν_6, ν_{24}, and ν_{50}. ν_0 consists of CO bending at the OH groups of C_1 and C_4, and CH bending at C_5. ν_6 involves OH bending at C_3 and CH bending at C_2 and C_5. ν_{24} is a combination of CH bending at C_2, C_3, and C_4. ν_5 consists of CO bending and OH stretching at C_3.

To gain insight into the mechanism of the dissociative photoionization, we carried out ab initio molecular dynamics (AIMD) calculations with B3LYP/6-31+G(d,p), starting from initial structures that are slightly displaced along the most FC-active modes described above. We notice that significant fragmentation occurs within 4 ps (with a 2 fs time step at 300K). At this time scale, the most active fragmentation channels are those that produce neutral H_2O (m/z 116) and CH_2O (m/z 104, 86, 60 and 44, see SM for chemical structures). m/z 104 is produced by CH_2O elimination, while the m/z 86, 60 and 44 fragments are formed by secondary fragmentation following CH_2O elimination. Another channel that we observed is the elimination of CH_3O (m/z 103). Experimentally, apart from m/z 104, all the other fragments have been observed. However, strong signals observed at m/z 70 and 73 are not reproduced by the simulations. Previous experiments[13] show the presence of m/z 104, 86, 60 and 44 (which are predicted by AIMD). Since only 50 trajectories were run, it is unrealistic to expect to observe all possible fragmentation channels in these limited simulations. Moreover, we did not perform an exhaustive investigation of secondary fragmentation channels. A possibility for the presence of m/z 70 and 73 could be that these are formed by ionization of neutral fragments which have been formed thermally, and not from dissociative photoionization.

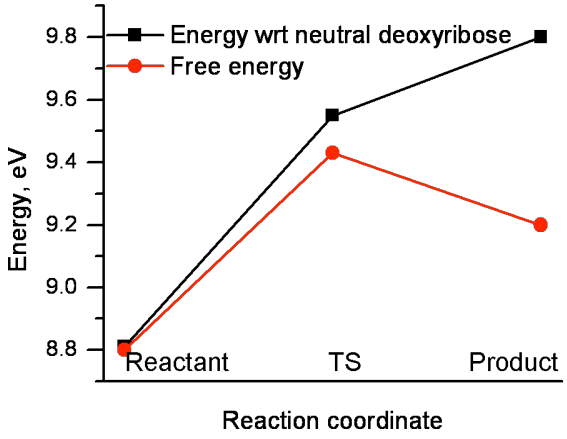

Figure 5: The free energy along the reaction coordinate of the constrained optimized structures taken from AIMD snapshots. Entropy contribution was evaluated within the RRHO approximation.

We further analyze the H_2O elimination fragmentation channel. The AIMD trajectories reveal that most of the processes start with the C_4-C_5 bond breaking, in accordance with our expectations. Since the C_4-C_5 bond is significantly weakened in the cation (as evidenced by its elongated bond length of 1.84 Å), it is most likely to break causing the cyclic structure to unfurl. This allows the OH groups on C_3 and C_1 to come close to each other, which is promptly followed by water elimination. The reaction can be monitored by observing the time evolution of the C_4-C_5 bond length as well as the OH bond lengths (see SM). To understand the nature of the reaction barrier, we take snapshots from the MD trajectories and perform constrained optimization (such calculations yield energy profile along an approximate reaction coordinate). During the ring-opening part of the trajectory, the reaction coordinate is approximated by C_4-C_5 distance (which is, therefore, frozen in optimizations), whereas the second part (water elimination facilitated by the OH groups on C_3 and C_1 approaching each other) is represented by the O-H bond length of the C_1 carbon. Figure 5 shows the free energy change from the neutral deoxyribose (calculated from the energy of the constrained optimized structures and the entropy within the rigid-rotor-harmonic-oscillator, RRHO, approximation) at the reactant, product and transition state (TS). The energy along the reaction coordinate increases, since it is dominated by bond-breaking (C_4-C_5, C_3-O, C_1O-H bond breaks and one OH bond is formed), which is

endothermic. However, the entropy increase leads to negative free energy change. The computed approximate minimum energy path suggests that the rate-determining step is the bond breaking and subsequent opening up of the ring (~9.4+/- 0.5 eV barrier), which is in excellent agreement with the experimental threshold for water elimination. It also shows the structure of the reactant, product, and the TS. A detailed picture of the process along the reaction coordinate is included in the SM. It shows that since the ring opening and fragmentation processes are strongly affected by the entropy change, the energy and the free energy profiles are significantly different from each other. A movie of the water elimination channel is also included in the SM. These approximate calculations of the minimum energy path were validated by computing fully optimized TS, which yielded a very similar structure and a ~9.8 eV barrier.

To conclude, we have measured an experimental adiabatic ionization energy of 9.1 eV for deoxyribose in the pyranose form in the gas phase, and this value agrees well with a theoretical estimate of 8.8 eV. Electronic structure and AIMD calculations provide insight into the water elimination pathway upon deoxyribose dissociative photoionization and the calculated 9.4-9.8 eV barrier agrees well with experimental observations. This combined experimental and theoretical approach in studying the dissociative photoionization of a model sugar will find application in studying biomass decomposition where VUV photoionization mass spectrometry is being proposed as a tool for chemical analysis. The calculations will aid the design of future experiments to probe the dynamics of the dissociative photoionization using ion-electron coincidence or ultra-fast pump probe experiments with VUV photons.

Experimental and computational:

The experiments were performed at the Chemical Dynamics Beamline at the Advanced Light Source (SM). Deoxyribose was gently desorbed via thermal heating and subsequently ionized by tunable VUV synchrotron radiation and extracted into a reflectron time-of-flight (TOF) mass spectrometer. A TOF mass spectrum is recorded at photon energies between 8.5-11.0 eV, with 50 meV resolution and photoionization efficiency curves are extracted from these data sets. The optimized geometries of the pyranose and furanose form of 2-deoxy-D-ribose were calculated by density functional theory (DFT) with the ωB97x functional[24] and the cc-pVTZ basis set[25] to identify the most stable structure in the gas phase. The optimized structures of the cationic species were calculated at the same level of theory. The vertical and adiabatic ionization energies

were computed with DFT as well as EOM-IP-CCSD[26-31] using the same basis set. The fragmentation dynamics of the cationic species was analyzed using AIMD simulations with the B3LYP functional[32,33] and the 6-31+G(d,p) basis set. The water elimination channel (which was found experimentally to be one of the dominant channels) was further studied by optimizing the structures with constraints (at the ωB97x/cc-pVTZ level) along the reaction path obtained from AIMD snapshots. The entropic effects were calculated within the RRHO approximation to estimate the barrier for the water elimination process. All calculations were performed using the Q-Chem electronic structure program[34].

Acknowledgements

This work is supported by the Office of Science, Office of Basic Energy Sciences, of the US Department of Energy under Contract No. DE-AC02-05CH11231, through the Chemical Sciences Division (A.G., L.K.T. M.A., and the Advanced Light Source), and DE-FG02-05ER15685 (A.I.K.). The calculations were conducted using resources of the iOpenShell Center for Computational Studies of Electronic Structure and Spectroscopy of Open-Shell and Electronically Excited Species (iopenshell.usc.edu) supported by the National Science Foundation through the CRIF:CRF CHE-0625419+0624602+0625237.

Supporting Information Available: Theoretical description of the structure and character of the deoxyribose cation, calculation of the water elimination channel for fragmentation, movie of the water elimination channel, calculated photoelectron spectrum, and experimental photoionization efficiency curves of major fragments, and optimized geometries of deoxyribose. This material is available free of charge via the Internet at http://pubs.acs.org

References

(1) Guler, L. P.; Yu, Y. Q.; Kenttamaa, H. I. J. Phys. Chem. A **2002**, 106, 6754.

(2) Shukla, M. K.; Leszczynski, J. In Radiation Induced Molecular Phenomena in Nucleic Acids; Shukla, M. K., Leszczynski, J., Eds.; Springer: 2008, p 1.

(3) Baccarelli, I.; Gianturco, F. A.; Scifoni, E.; Solov'yov, A. V.; Surdutovich, E. Eur. Phys. J. D **2010**, 60, 1.

(4) Ptasinska, S.; Denifl, S.; Scheier, P.; Mark, T. D. J. Chem. Phys. **2004**, 120, 8505.

(5) Shin, J.-W.; Dong, F.; Grisham, M. E.; Rocca, J. J.; Bernstein, E. R. Chem. Phys. Lett. **2011**, 506, 161.

(6) Alvarado, F.; Bernard, J.; Li, B.; Bredy, R.; Chen, L.; Hoekstra, R.; Martin, S.; Schlatholter, T. Chemphyschem **2008**, 9, 1254.

(7) Colson, A. O.; Besler, B.; Sevilla, M. D. J. Phys. Chem. **1993**, 97, 8092.

(8) Slavicek, P.; Winter, B.; Faubel, M.; Bradforth, S. E.; Jungwirth, P. J. Am. Chem. Soc. **2009**, 131, 6460.

(9) Dampc, M.; Mielewska, B.; Siggel-King, M. R. F.; King, G. C.; Zubek, M. Chem. Phys. **2009**, 359, 77.

(10) Milosavljevic, A. R.; Kocisek, J.; Papp, P.; Kubala, D.; Marinkovic, B. P.; Mach, P.; Urban, J.; Matejcik, S. J. Chem. Phys. **2010**, 132.

(11) Baccarelli, I.; Gianturco, F. A.; Grandi, A.; Sanna, N. Int. J. Quantum Chem. **2008**, 108, 1878.

(12) Baccarelli, I.; Gianturco, F. A.; Grandi, A.; Sanna, N.; Lucchese, R. R.; Bald, I.; Kopyra, J.; Illenberger, E. J. Am. Chem. Soc. **2007**, 129, 6269.

(13) Vall-Ilosera, G.; Huels, M. A.; Coreno, M.; Kivimaki, A.; Jakubowska, K.; Stankiewicz, M.; Rachlew, E. Chemphyschem **2008**, 9, 1020.

(14) Huber, G. W.; Iborra, S.; Corma, A. Chem. Rev. **2006**, 106, 4044.

(15) Lin, Y. C.; Cho, J.; Tompsett, G. A.; Westmoreland, P. R.; Huber, G. W. J. Phys. Chem. C **2009**, 113, 20097.

(16) Bahng, M. K.; Mukarakate, C.; Robichaud, D. J.; Nimlos, M. R. Anal. Chim. Acta **2009**, 651, 117.

(17) Kostko, O.; Takahashi, L. K.; Ahmed, M. Chem. Asian J. **2011**, (In press)

(18) Zhou, J.; Takahashi, L. K.; Wilson, K. R.; Leone, S. R.; Ahmed, M. Anal. Chem. **2010**, 82, 3905.

(19) Takahashi, L. K.; Zhou, J.; Kostko, O.; Golan, A.; Leone, S. R.; Ahmed, M. J. Phys. Chem. A **2011**, 115, 3279.

(20) Ghosh, D.; Isayev, O.; Slipchenko, L. V.; Krylov, A. I.; J. Phys. Chem. A **2011**, 115, 6028.

(21) Mozhayskiy, V. A.; Krylov, A. I.; ezSpectrum, http://iopenshell.usc.edu/downloads.

(22) Khistyaev, K.; Bravaya, K. B.; Kamarchik, E.; Kostko, O.; Ahmed, M.; Krylov, A. I. Faraday Discuss. **2011**, 150, 313.

(23) Bravaya, K. B.; Kostko, O.; Dolgikh, S.; Landau, A.; Ahmed, M.; Krylov, A. I.; J. Phys. Chem. A **2010**, 114, 12739.

(24) Chai, J.-D.; Head-Gordon, M.; J. Chem. Phys. **2008**, 128, 084106.

(25) Dunning, T. H.; J. Chem. Phys. **1989**, 90, 1007.

(26) Sinha, D.; Mukhopadhyay, D.; Mukherjee, D.; Chem. Phys. Lett. **1986**, 129, 369.

(27) Pal, S.; Rittby, M.; Bartlett, R. J.; Sinha, D.; Mukherjee, D.; Chem. Phys. Lett. **1987**, 137, 273.

(28) Stanton, J. F.; Gauss, J. J.; J. Chem. Phys. **1994**, 101, 8938.

(29) Pieniazek, P. A.; Arnstein, S. A.,; Bradforth, S. E.; Krylov, A. I.; Sherill, C. D.; J. Chem. Phys. **2007**, 127, 164110.

(30) Pieniazek, P. A.; Bradforth, S. E.; Krylov, A. I.; J. Chem. Phys. **2008**, 129, 074104.

(31) Krylov, A. I.; Annu. Rev. Phys. Chem. **2008**, 59, 433.

(32) Becke, A. D.; Phys. Rev. A **1988**, 38, 3098.

(33) Lee, C. T.; Yang, W. T.; Parr, R. G.; Phys. Rev. B **1988**, 37, 785.

(34) Shao, Y.; Molnar, L. F.; Jung, Y.; Kussmann, J.; Ochsenfeld, C.; Brown, S.; Gilbert, A. T. B.; Slipchenko, L. V.; Levchenko, S. V.; O'Neil, D. P.; Distasio, R. A., Jr.; Lochan, R. C.; Wang, T.; Beran, G. J. O.; Besley, N. A.; Herbert, J. M.; Lin, C. Y.; Van Voorhis, T.; Chien, S. H.; Sodt, A.; Steele, R. P.; Rassolov, V. A.; Maslen, P.; Korambath, P. P.; Adamson, R. D.; Austin, B.; Baker, J.; Bird, E. F. C.; Daschel, H.; Doerksen, R. J.; Drew, A.; Dunietz, B. D.; Dutoi, A. D.; Furlani, T. R.; Gwaltney, S. R.; Heyden, A.; Hirata, S.; Hsu, C.-P.; Kedziora, G. S.; Khalliulin, R. Z.; Klunziger, P.; Lee, A. M.; Liang, W. Z.; Lotan, I.; Nair, N.; Peters, B.; Proynov, E. I.; Pieniazek, P. A.; Rhee, Y. M.; Ritchie, J.; Rosta, E.; Sherrill, C. D.; Simmonett, A. C.; Subotnik, J. E.; Woodcock, H. L., III; Zhang, W.; Bell, A. T.; Chakraborty, A. K.; Chipman, D. M.; Keil, F. J.; Warshel, A.; Herhe, W. J.; Schaefer, H. F., III; Kong, J.; Krylov, A. I.; Gill, P. M. W.; Head-Gordon, M.; Phys. Chem. Chem. Phys. **2006**, 8, 3172.